Materials & Design 238 (2024) 112639

Contents lists available at ScienceDirect

Materials & Design

journal homepage: www.elsevier.com/locate/matdes

A novel natural polysaccharide dissolving microneedle capable of adsorbing pus to load EGCG for the treatment of acne vulgaris

Junbo Zhang [a,1], Peng Guo [a,1], Mengyu Qiu [a], Guofeng Zhong [a], Qin Yang [a], Pengkun Lei [a], Kaijun Gou [b,c], Rui Zeng [b,c,*], Chen Zhang [a,*], Yan Qu [a,*]

[a] State Key Laboratory of Southwestern Chinese Medicine Resources, School of Pharmacy, Chengdu University of Traditional Chinese Medicine, Chengdu 611137, China
[b] College of Pharmacy, Southwest Minzu University, Chengdu 610041, China
[c] Key Laboratory of Research and Application of Ethnic Medicine Processing and Preparation on the Qinghai Tibet Plateau, Chengdu 610225, China

ARTICLE INFO

Keywords:
Acne vulgaris
Microneedle
Bletilla striata polysaccharide
Epigallocatechin gallate
Propionibacterium acnes
Diatomaceous earth

ABSTRACT

Acne vulgaris is a common inflammatory skin disease associated with Propionibacterium acnes *(P. acnes)*, with serious physical and psychological effects on patients. Conventional topical use of antibiotics is not effective due to the skin barrier and oral administration can adversely affect the intestinal flora. Microneedle is a novel type of localized drug delivery system that noninvasively breaks through the stratum corneum barrier and effectively enhances the transdermal absorption of drugs. Here, *Bletilla striata* polysaccharide (BSP)/Hyaluronic acid (HA) loaded Epigallocatechin gallate (EGCG) was used as the microneedle body to easily penetrate the epidermis and enhance antibacterial ability. Polyvinyl alcohol (PVA) and Diatomaceous earth (DE) are used as the microneedle backing to absorb pus and bacterial debris, prevent re-infection of bacteria and promote skin healing. Compared to traditional antibiotics, the excellent skin permeability of EGCG@BSP/HA MNs studied here can improve the efficacy and solve side effects and drug resistance. In vivo studies in mice models induced by *P. acnes* showed that this microneedle could effectively reduce skin swelling, inhibit bacterial growth and reduce the levels of TNF-α, IL-8 and MMP-2. In summary, this study provides an ideal antimicrobial drug delivery system for the treatment of acne vulgaris.

1. Introduction

Acne vulgaris is a common skin disorder associated with sebaceous glands that affects more than 80 % of the world's population [1,2]. Acne can be triggered by a variety of different factors (e.g., genetics, hormones, infections, and the environment), and *P. acnes* infections are the main cause of acne [3]. This is due to excessive sebum production by the sebaceous glands blocking the sebaceous glands of the hair follicles, leading to a lack of oxygen in the microenvironment, promoting the growth and reproduction of *P. acnes*, which in turn triggers acne. The lipase of *P. acnes* can catalyze the hydrolysis of sebum triglycerides into free fatty acids, thereby destroying the follicular epithelium. Some chemokines secreted by it will also attract immune cells to the sebaceous glands of hair follicles, thereby stimulating the production of pro-inflammatory cytokines. In addition, these cellular damage, metabolic by-products, and bacterial debris can cause rapid growth of *P. acnes* and aggravate the inflammatory response [4]. The pus in acne vulgaris is mainly composed of sebaceous gland secretions (fatty acids), white blood cells, necrotic cells, bacterial remnants and their metabolites, and tissue fluid [5–7]. Acne can also leave behind hard-to-heal scars, which can have a serious physical and psychological impact on the patient [8]. At present, the treatment of acne vulgaris caused by *P. acnes* is mainly based on the use of antibiotics, including oral antibiotics or topical use of antibiotic ointment [9]. However, due to the barrier effect of the skin, most medications cannot be delivered through the skin to achieve therapeutic effects, and oral medications can be harmful to the intestinal flora [10,11]. Therefore, it is crucial to create a transdermal in situ medicine delivery system that increases skin permeability in order to cure acne vulgaris.

In recent years, microneedles have been extensively studied due to their special morphology and excellent performance [12]. As a new minimally invasive transdermal drug delivery system, microneedle is the application of micro-processing technology and made of micron-sized microneedle array [13]. It can penetrate the stratum corneum of

* Corresponding authors.
E-mail addresses: rzeng@swun.edu.cn (R. Zeng), chenzhang_1990@126.com (C. Zhang), quyan028@126.com (Y. Qu).
[1] These authors have contributed equally to this work.

https://doi.org/10.1016/j.matdes.2024.112639
Received 29 August 2023; Received in revised form 29 December 2023; Accepted 3 January 2024
Available online 8 January 2024

the skin, improve the release rate and bioavailability of the drug, and overcome the disadvantages of slow bioavailability of traditional patches. The microneedle will not stimulate the subcutaneous pain nerve, will not cause damage to the skin, will not cause pain when administered, and the patient 's compliance is greatly improved. The microneedles have been available in dissolving, solid, coated, hollow, and hydrogel-based microneedles [14]. Dissolving microneedles are made of hydrophilic and biocompatible polymers, which can penetrate the stratum corneum into the epidermis/ dermis to create microchannels, so that the drug can be continuously and stably transported to the skin and dissolved in contact with the skin interstitial fluid to effectively load and release the related drugs [15,16]. In the treatment of acne, the microneedles can physically pierce the acne pustules and discharge the pus, so as to achieve simple debridement [17,18]. Compared to oral antibiotics, dissolving microneedles deliver lower doses, provide better efficacy, and avoid the side effects of oral administration. Therefore, dissolving microneedles have attracted widespread attention because of their biosafety, accuracy and ease of administration, and can be used for in situ administration of painless acne treatment [19–21].

BSP is a natural soluble polymer extracted from *Bletilla striata*, consisting of α-mannose, β-mannose, and β-glucose [22]. Because of its biological solubility, stability and biodegradability, it is recognized as an excellent biomaterial for medicine [23–25]. BSP has been studied to have the activities of promoting wound healing, hemostasis, anti-inflammation, anti-oxidation and immune regulation [24,26]. Our research team has dedicated efforts towards the development of BSP as a biomaterial for many applications, and has obtained the preliminary application prospect of BSP in the preparation of dissolving microneedles [27–32].

EGCG is one of the natural polyphenol catechins in green tea with broad-spectrum, highly effective antibacterial, antioxidant, and anti-inflammatory effects [33–35]. Studies have shown that EGCG can inhibit the proliferation and lipid synthesis of sebaceous gland cells, induce cell cycle arrest and apoptosis, inhibit the production of inflammatory cytokines and the proliferation of *P. acnes* in the treatment of acne [36–38].

In this study, in order to enhance the performance of microneedles and reduce side effects, the microneedle body is a BSP/HA composite material loaded with EGCG. When the microneedle penetrates the epidermis into the dermis, it is dissolved in contact with the interstitial fluid of the skin, and can release of EGCG in the acne infection lesion, thus effectively inhibiting the bacteria. BSP has a good healing effect and can promote wound healing at the site of infection. PVA/DE is used as a backing matrix for microneedles, which can adsorb pus and other purulent exudates and bacterial debris to promote healing and prevent further infection [39–41]. Subsequently, the mechanical properties, skin insertion ability, dissolution properties and drug distribution of the EGCG@BSP/HA MNs were studied. The acne model was induced by intradermal injection of *P. acnes* in the back of mice to observe the therapeutic effects of EGCG@BSP/HA MNs on acne and their effects on the levels of inflammatory factors. We were able to demonstrate that this soluble microneedle patch with skin-penetrating and adsorption capabilities can effectively deliver antimicrobial drugs to the lesion and inhibit *P. acnes* to effectively treat acne vulgaris in situ, providing reliable evidence that the novel delivery system is effective in the treatment of acne vulgaris (Fig. 1).

2. Materials and methods

2.1. Materials

Epigallocatechin gallate (EGCG) was purchased from Chengdu Chroma-Biotechnology Co., Ltd. (Chengdu, China). Sodium hyaluronate (HA, MW < 10 kDa) was provided by Huaxi Biotechnology Co., Ltd. (Shandong, China). Polyvinyl alcohol (PVA) (purity, ≥98 %) was obtained from Chengdu Kelon Chemical Reagent Co., Ltd. (Chengdu, China). Phosphoric acid, acetonitrile, and the chromatographic grades of methanol used in this study were purchased from Sigma-Aldrich Co., Ltd. (Shanghai, China).

2.2. Animals

The male ICR mice (8 weeks old; 20 ~ 25 g) were procured from SPF Biotechnology Co., Ltd. (Beijing, China). All animals were housed under standardized environmental and nutritional conditions (ambient temperature maintained at 23 ± 2 °C; relative humidity at 55 ± 5 %; with a light/dark cycle of 12 h) and underwent a period of acclimatization and feeding for seven days prior to the commencement of the experiment. All animal experiments were conducted in accordance with the approval granted by the Animal Ethics Committee of Chengdu University of Traditional Chinese Medicine.

2.3. Preparation of BSP

The optimal extraction and purification process for BSP has been obtained by extensive experiments in the laboratory [30]. In short, the crude BSP was first obtained by degreasing, water extraction, deproteinization, alcohol precipitation and other steps, and then purified by DEAE-52 cellulose column (6.0 cm × 55.0 cm) to prepare refined BSP for subsequent use [27–30]. In addition, our team carried out a more detailed characterization of BSP and determined the total

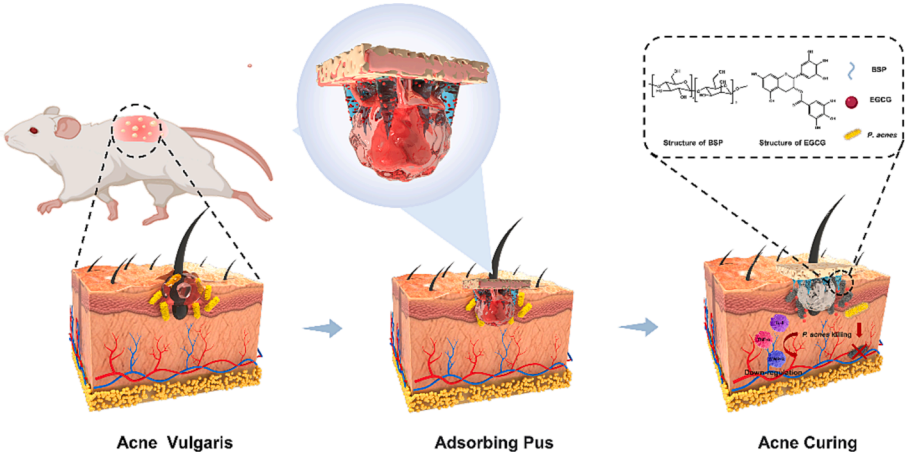

Fig. 1. Schematic diagram of EGCG@BSP/HA MNs treatment for acne vulgaris.

polysaccharide content of BSP using the phenol–sulfuric acid method according to the UV–visible spectrophotometric method (General rule 0401) [42]; The homogeneity and molecular weight of BSP were determined by high performance gel permeation chromatography (HPGPC). The monosaccharide composition of BSP was identified using the PMP (3-methyl-1-phenyl-5-pyrazolone) labeling method [32,43].

2.4. Preparation of EGCG@BSP/HA MNs patches

In this experiment, EGCG@BSP/HA MNs were prepared by two-step centrifugation (Fig. 2A). The mold was prepared with flexible polydimethylsiloxane (PDMS). First, 90 mg of EGCG was dissolved in 3 mL of pure water, fully stirred and dissolved, and then 150 mg of BSP and 150 mg of HA were added, and the mixture was completely stirred and swelled. The prepared solution was poured into the microneedle mold, centrifuged at 3500 rpm for 25 min at 25 °C to form a body of the microneedle needle, and the excess liquid loaded with drug on the mold was gently scraped. 150 mg of PVA were fully dissolved in 1 mL of pure water, and 25 mg of DE was added and well stirred. The suspension of PVA and DE was poured into the microneedle mold, and centrifuged at 3000 rpm for 5 min at 25 °C to form the backing of the microneedle. The mold was then dried for 24 h at 37 °C in an oven, and the microneedles were taken out and placed in a drier with tainted silica gel. BSP/HA MNs were prepared in this way, but without the addition of EGCG. FITC-labeled microneedles have also been prepared in this way.

2.5. Characterization of EGCG@BSP/HA MNs

2.5.1. Morphology of EGCG@BSP/HA MNs

The appearance of the microneedles was evaluated by optical microscopy (CX21, Olympic) and scanning electron microscopy (SEM) (SU9010, Hitachi, Japan). To comprehend the medication distribution and 3D structure in microneedles, MNs labeled with FITC as a fluorescent chromogen were prepared and evaluated by laser confocal microscopy.

2.5.2. Mechanical strength of EGCG@BSP/HA MNs

The mechanical strength of EGCG@BSP/HA MNs was analyzed by using the Texture Analyzer (Motion-pro, China). A 5 × 5 microneedle array was positioned onto the designated test region. A cylindrical probe with a diameter of 6 mm, was then introduced and the microneedles were subjected to compression at a rate of 5 mm/min. This compression continued until the tip of the microneedles either fractured or experienced displacement up to a distance of 900 μm. The sensor displacements and forces of the EGCG@BSP/HA MNs are also recorded [44].

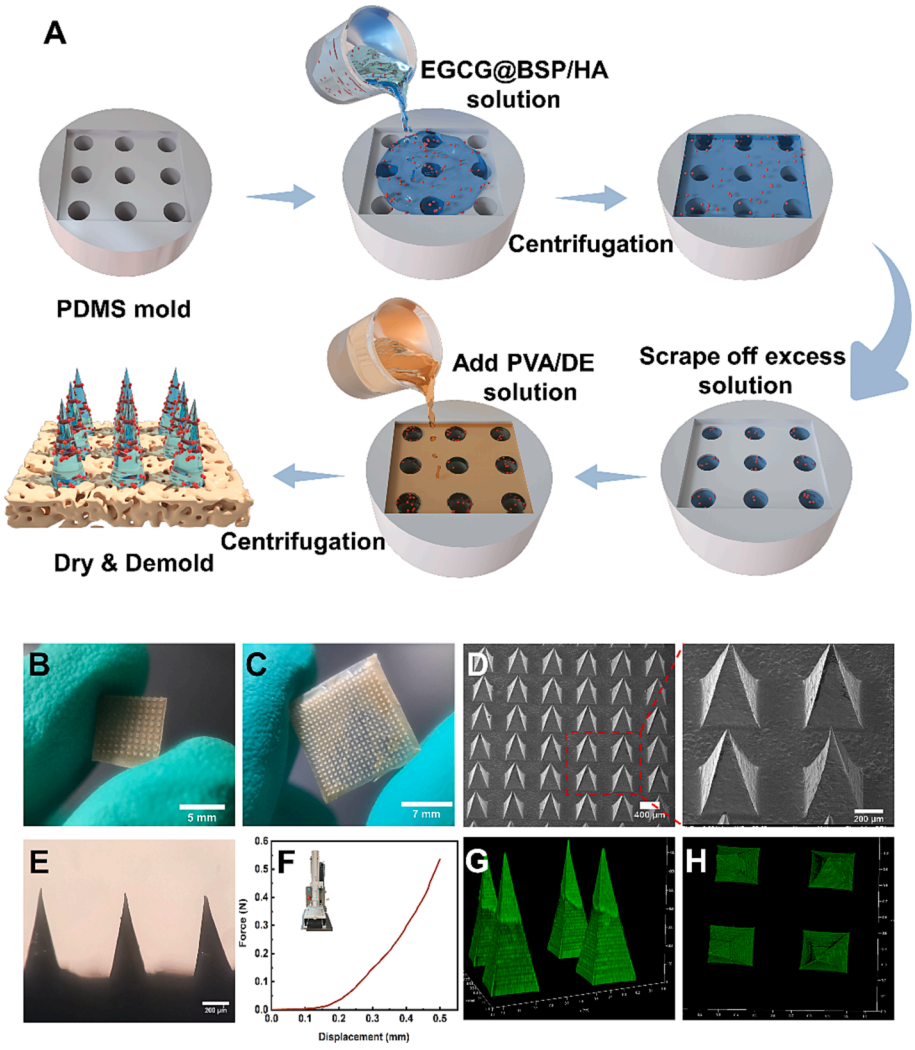

Fig. 2. Preparation and characterization of EGCG@BSP/HA MNs. (A) Schematic diagram of the preparation process of EGCG@BSP/HA MNs. (B) and (C) Photograph of representative EGCG@BSP/HA MNs patch. (D) SEM image of EGCG@BSP/HA MNs. (E) Optical microscope image of EGCG@BSP/HA MNs (Scale bar: 200 μm). (F) Force-distance curve showing the mechanical strength of EGCG@BSP/HA MNs. (G) Side view of 3D reconstructed image of Rg3-MNs captured by CLSM. (H) Top view of 3D reconstructed image of EGCG@BSP/HA MNs captured by CLSM.

2.5.3. EGCG content in EGCG@BSP/HA MNs

The microneedle body and backing of EGCG@BSP/HA MNs were separated using a scalpel and the body of the needle was dissolved in 1 mL of pure water, and after it was completely dissolved, the emulsion was broken by dissolving it with 2 times volume of 50 % methanol. The samples need to be filtered through 0.22 μm microporous membrane. The content of EGCG in the microneedles was determined by high performance liquid chromatography (HPLC). High performance liquid chromatography (HPLC; Thermo Scientific Ultimate3000, USA) was performed on a C18 column (Thermo Scientific, 250 × 4.6 mm, USA) with the mobile phase of acetonitrile-0.2 % phosphoric acid in water (0–8 min, 8:92; 8–28 min, 8:92 ~ 22:78; 28–29 min,22:78 ~ 8:92; 29–34 min, 8:92, V/V) at a flow rate of 0.75 mL/min, and the absorption peak of EGCG was observed at a wavelength of 272 nm. The content of EGCG in the microneedles was calculated from the standard curve ($y = 266.75x-21.012$, $R^2 = 0.9968$).

2.6. Insertion test of EGCG@BSP/HA MNs

2.6.1. In vitro and vivo insertion test

Parafilm M® was used as a skin mimic to evaluate the in vitro insertion properties of EGCG@BSP/HA MNs. Specifically, the Parafilm M® film was folded into ten layers and placed on a stainless steel plate, the EGCG@BSP/HA MNs were attached to the removable test probes with double-sided tape, and the probes with the microneedles were pressed against the folded Parafilm M® film with the required force of 30 N. Then, the EGCG@BSP/HA MNs patches were removed from the Parafilm M® films, and the number of microchannels created by the EGCG@BSP/HA MNs on each layer of Parafilm M® films was observed with an optical microscope and the rate of inserted holes was calculated.

The skin insertion ability of microneedles was tested on the dorsal skin of ICR mice. Before the experiment, the hair on the back of the mice was removed and the shaved area was about 2 cm × 2 cm. Following a period of skin recovery, the surface of the skin was sterilized using alcohol. Subsequently, the microneedle was inserted into the skin and left in place for a duration of 5 min. The treated skin was then incised, fixed using a 4 % paraformaldehyde solution for a period of 48 h, embedded in paraffin, and subjected to staining with hematoxylin and eosin (H&E). Finally, the sections were observed under a light microscope (DM750, Leica, Germany).

2.6.2. Skin irritation recovery test of EGCG@BSP/HA MNs and TEWL measurement

To assess the skin irritation induced by the insertion of microneedles, a microneedle patch was inserted into the dorsal skin of ICR mice after depilation and held for 5 min before being removed. The treated areas were also photographed with a camera at 0, 5, 10, 15, 20, 25 and 30 min after removal to observe the recovery of the skin.

In order to investigate the impairment and restoration of the skin barrier, we employed the Delfin VapoMeter® (Delfin Technologies ltd., Kuopio, Finland) to measure the rate of Trans Epidermal Water Loss (TEWL). TEWL values before and after insertion of EGCG@BSP/HA MNs into the skin were recorded until they returned to the baseline values, meaning the process of closing the skin and the subsequent restoration of barrier function. Hair removal mice without EGCG@BSP/HA MNs insertion were used as the control group.

2.6.3. In vivo dissolution of EGCG@BSP/HA MNs

The dorsal dermal skin of ex-vivo depilated ICR mice was fixed on a foam plate, and the microneedles were inserted into the skin and removed at 0 min, 5 min, 10 min and 15 min, and the obtained microneedles were imaged using an optical microscope to observe the residual tip length. The complete tip height of the microneedle should be observed and recorded before it is inserted into the skin of mice.

2.7. In vitro biodistribution of EGCG@BSP/HA MNs

2.7.1. In vitro penetration depth study of EGCG@BSP/HA MNs

Fluorescein isothiocyanate (FITC) labeled microneedles were selected to further evaluate the transdermal penetration ability of drug-loaded microneedles. First, the ICR mice were anesthetized and shaved. The fluorescent FITC-loaded microneedle patches were inserted into the skin of the mice, pressed for 10 min, and covered with tape for 30 min. The mice that underwent treatment were euthanized, and the treated skin was extracted and subjected to scanning using a confocal laser scanning microscope (CLSM) at various Z-axis levels. A fluorescent signal was detected at 488 nm, allowing observation of the degree of penetration of the microneedle. Scanning was performed every 20 μm depth until no fluorescence signal was detected, and lastly, subsequent to the determination of the uppermost and lowermost values of the height along the Z-axis that were captured by the Confocal Laser Scanning Microscope (CLSM), images were obtained from the XY plane with a gradual increase in Z-axis height. The 3D reconstructed images were obtained by overlapping the XY plane images at different Z-axis heights.

2.7.2. In vitro transdermal delivery ability of EGCG@BSP/HA MNs

In vitro transdermal administration of EGCG@BSP/HA MNs was studied using a Franz diffusion cell [45]. EGCG@BSP/HA MNs were inserted into the skin surface of isolated mice and held in place by a medical surgical membrane. The skin containing EGCG@BSP/HA MNs was placed on the receiving cell using a magnetic stirrer. 8 mL of saline containing 20 % ethanol treated with ultrasound was added to the receiving cell chamber as the receiving medium, and air bubbles under the skin were drained so that the receiving medium was in full contact with the skin. The device was put in a thermostatic water bath set at 37.5 ± 0.5 °C with 300 rpm of agitation to simulate in vivo release conditions. 600 μL of acceptor solution was removed from the receiving cell at specified time intervals and isothermal and equal volume of receiving medium was added at the same time, and three experiments were performed in parallel for each group. The removed fresh receiver solution was blown dry with nitrogen and then 100 μL of 50 % methanol was added to re-dissolve the solution, and the concentration of EGCG in the receiver solution was determined by high performance liquid chromatography (HPLC).

2.8. The hemolysis test of EGCG@BSP/HA MNs

The blood compatibility of EGCG@BSP/HA MNs was evaluated using an in vitro hemolysis test. A piece of EGCG@BSP/HA MNs and A piece of BSP/HA MNs were taken, added to 10 mL of saline, and immersed in a biochemical incubator at 37 °C for 48 h. The erythrocytes were isolated by centrifugation of venous blood from the ear margins of New Zealand White rabbits at 2000 rpm for 10 min, and then washed three times with saline. The purified erythrocytes were diluted with saline to obtain RBC suspension (5 %, v/v). For this study, the negative saline control and the positive 0.1 % Triton X-100 control were selected. 0.5 mL of microneedle extract, 0.5 mL of negative control and 0.5 mL of positive control were added to a 2 mL centrifuge tube. Then, 0.3 mL of fresh diluted blood was added to each tube and the tubes were heated in a 37 °C bath for 1 h. Preparation of 200 μL of RBC suspension (5 %, v/v), mixed with 800 μL of 0.9 % NaCl solution as a negative control. A 200 μL RBC suspension was prepared and mixed with 800 μL of 0.1 % Triton X-100 (T8200, Solarbio) as a positive control. 200 μL of RBC suspension was prepared and mixed with 100 μL of microneedle mix and 700 μL of 0.9 % NaCl solution as experimental group. The tubes were incubated at 37 °C for 1 h. The tubes were centrifuged at 1500 rpm for 5 min to absorb the supernatant and absorbance was measured at 540 nm [46,47].

$$\text{Hemolysis rate}\ (\%) = 100\% \times \left(\text{OD}_{\text{sample}} - \text{OD}_{\text{negative control}}\right) / \left(\text{OD}_{\text{positive control}} - \text{OD}_{\text{negative control}}\right) \quad (1)$$

2.9. In vitro cytotoxicity of EGCG@BSP/HA MNs

The cytocompatibility of the microneedles was evaluated by CCK-8 assay [48]. First, DE-free microneedles were prepared as EGCG@BSP/HA MNs 1 and DE-containing microneedles as EGCG@BSP/HA MNs 2 according to the method of 2.4. 10 mg of sterilized EGCG@BSP/HA MNs1, EGCG@BSP/HA MNs 2, and BSP/HA MNs were immersed in 10 mL of DMEM complete medium containing 10 % fetal bovine serum and 1 % double antibody, and then extracted at 7 °C for 24 h to obtain the concentration of 10 mg/mL of the extract. And they were diluted to concentrations of 0.25 mg/mL, 0.5 mg/mL and 1 mg/mL co-culture medium. L929 cells in logarithmic growth phase were inoculated in 96-well plates at a concentration of 5×10^4 cells/mL. Cells were cultured for 24 h and then the medium was changed to co-culture solution, The control group was further cultured with fresh medium, and the blank group was cultured with fresh medium in wells without cells. The cells were incubated in a sterile incubator at 37 °C with 5 % CO_2 for 24 h and 48 h. CCK-8 reagent was then added according to the manufacturer's method and absorbance (OD) was measured using a microplate reader. Each sample was paralleled six times. Cell viability was calculated by the formula:

$$\text{Cell viability}(\%) = \left(\text{OD}_{\text{sample}} - \text{OD}_{\text{blank}}\right) / \left(\text{OD}_{\text{control}} - \text{OD}_{\text{blank}}\right) \times 100\% \quad (2)$$

2.10. The adsorption properties of DE

The structure of DE was observed by scanning electron microscope (SEM). The adsorption capacity of DE on tiny molecules was evaluated by adding 0, 5, 25, 50 and 100 mg of DE in centrifuge tubes, and an equal amount of rhodamine solution in each centrifuge tube, mixing thoroughly and then centrifuging the tubes at 4000 rpm for 15 min. Oleic acid spiked with Rhodamine was mixed with different masses of DE and Activated Carbon (AC), to evaluate the adsorption capacity of DE for oil [41].

2.11. In vitro antibacterial effect of EGCG@BSP/HA MNs

Drug-loaded microneedles with different concentrations of EGCG were prepared according to the method of 2.4. A quarter of the above drug-loaded microneedles (10 × 10 arrays) were labeled as MNs 1, MNs 2, MNs 3, MNs 4, and MNs 5. The amount of EGCG loaded on them was determined as described in 2.5.3, which was 0, 21, 25, 33 and 45 μg/patch. The antibacterial properties of EGCG@BSP/HA MNs were evaluated using the dilution-coated plate method. The above microneedles with different EGCG concentration were placed at the bottom of 48-well plates, and 200 μL of *S. aureus* and *E. coli* bacterial solution (10^5 CFU/mL) were added and supplemented with 800 μL of liquid medium. The microneedles were cultured in a sterile incubator at 37 °C for 12 h. The bacterial solution was diluted with normal saline and 50 μL was applied to the agar plate. The sterile incubator was incubated at 37 °C for 24 h, and the photographs were taken. The number of colonies (n = 3) was calculated by ImageJ software. The bacteriostatic rate can be obtained by counting the bacterial population at the same dilution ratio [43,49].

The above microneedles with different EGCG concentration were placed at the bottom of 48-well plates, and 200 μL of *P. acnes* bacterial solution (10^5 CFU/mL) were added and supplemented with 800 μL of liquid anaerobic medium. The microneedles were incubated anaerobically with the bacterial solution in a sterile incubator at 37 °C for 48 h. The bacterial solution was diluted with normal saline and 50 μL was applied to the agar plate. The bacteria were incubated anaerobically in a sterile incubator at 37 °C for 48 h, and photographs were taken. The number of colonies (n = 3) was calculated by ImageJ software. The bacteriostatic rate can be obtained by counting the number of bacteria at the same dilution ratio.

$$\text{Antibacterial rate}(\%) = \left(\text{A}_{\text{negative control}} - \text{B}_{\text{sample}}\right) / \text{A}_{\text{negative control}} \times 100\% \quad (3)$$

The morphological changes of bacteria in the presence of EGCG@BSP/HA MNs were observed by scanning electron microscopy (SEM). *E. coli*, *S. aureus* and *P. acnes* were incubated with EGCG@BSP/HA MNs for 24 h at 37 °C, and those without microneedles were used as controls. The cultured bacterial solution was centrifuged at 4000 rpm, the supernatant was discarded, fixed with 2.5 wt% glutaraldehyde solution for 12 h, and then dehydrated with 10, 30, 50, 70, 90 and 100 % ethanol solution step by step for 15 min, and then centrifuged to discard the ethanol and freeze-dried, and the changes in the morphology of the bacteria were observed by scanning electron microscopy [50].

To better evaluate the antimicrobial properties of EGCG@BSP/HA MNs, they were compared to commercial microneedles (Fig. S1.) using the bacterial optical density [51]. The densities of *E. coli*, *S. aureus*, and *P. acnes* were adjusted to 10^8 CFU/mL, and 400 μL of each bacterial suspension was placed in a 24-well plate supplemented with 1.6 mL fresh medium with EGCG@BSP/HA MNs (array of 10 × 10, 45 μg) and a patch of commercia microneedles. *E. coli* and *S. aureus* were cultured at 37 °C for 12 h, and *P. acnes* was cultured at 37 °C for 48 h without oxygen. No microneedle samples were added to the control group. The above bacterial suspensions (200 μL/well) were collected and their optical density at 600 nm ($OD_{600\ nm}$) was determined by microplate reader. Each sample had three parallel group entries in each experiment.

2.12. In vivo anti-acne experiments of EGCG@BSP/HA MNs

Mice (ICR, male, 8 weeks, 25 ~ 30 g) were weighed and anesthetized. A shaver and depilatory cream were used to remove hair from the backs of the mice. After disinfecting the back skin of mice with a 75 % alcohol cotton ball, *P. acnes* (2×10^5 CFU/mL) was injected intradermally to establish an animal model of acne vulgaris [52–54]. On the second day, the mice were randomly divided into 5 groups of 5 mice each, model group (1 mL, coated with saline), BSP/HA MNs group (1/4 slice of drug-free microneedles), EGCG Solution group (1 mL, 45 μg/mL), and EGCG@BSP/HA MNs group (1/4 slice of microneedles, 45 μg), once a day for 4 consecutive days. The mice in the normal group did not receive modeling or any treatment [41,55].

During treatment, the thickness of the skin in the affected area of the acne was measured daily with a vernier caliper, and changes in the acne on the backs of the mice were photographed and recorded.

On the eighth day, all mice were euthanized. The skin was cut along the 2 mm edge of the incision, fixed with a 4 % paraformaldehyde solution, and next embedded in paraffin. The obtained tissue samples were subjected to staining using hematoxylin and eosin (H&E) in order to examine the process of skin thickening and the presence of inflammatory cell infiltration. Histologic examinations were performed using a pathology section scanner [56].

In addition, We also compared the anti-acne properties of EGCG@BSP/HA MNs and commercial microneedles in vivo. The animal model of acne vulgaris was established, administered and photographs were taken to document the changes in acne on the backs of the mice according to the above method. The commercial microneedles group (one slice of microneedles) was similarly administered continuously for 4 days.

2.13. Immunohistochemical analysis

The expression of the relevant proteins on the skin was detected by immunohistochemistry. The sections were placed in 3 % hydrogen peroxide solution (hydrogen peroxide:pure water = 1:9) to block endogenous peroxidase. The sections were added with primary antibody

and incubated at 4 °C overnight. After removing the sections, adding the secondary antibody that matches the primary antibody, and incubating for 30 min at 37 °C. The final step was adding a newly made diaminobenzidine color development solution. Under a microscope, when brownish-yellow positive particles form in the target tissue but no nonspecific color does, color development is halted with distilled water before counterstaining and mounting. The examination was performed using a pathology slide scanner.

2.14. Statistical analysis

The statistical disparities between the two groups were assessed by the use of an unpaired Student's *t*-test, while the statistical disparities across numerous groups were assessed using a one-way analysis of variance (ANOVA). The statistical calculations for all data were performed using the SPSS software. $P < 0.05$ was considered statistically significant. (* $P < 0.05$, ** $P < 0.01$, *** $P < 0.001$).

3. Results and discussion

3.1. Preparation of BSP

According to the results of the previous laboratory, according to the phenol–sulfuric acid method, the polysaccharide content of Bletilla striata polysaccharide was 63.46 %. The weight-average molecular weight (Mw) and number-average molecular weight (Mn) of BSP determined by HPGPC were 3.99×10^5 g/mol and 7.09×10^4 g/mol. Comparing the residence time of monosaccharide and standard in BSP, it was proved that BSP was a heteropolysaccharide, mainly composed of mannose and glucose, and the molar ratio was 2.946: 1. At the same time, the results of high acid salt oxidation, BSP is a β-d-mannose whose main chain is mainly (1 → 4) linked. In addition, the laboratory also used extensive FT-IR to analyze the chemical structure of BSP in detail, ^{1}H NMR and ^{13}C NMR spectral information, and even mapped the chemical structure of BSP [28–30].

3.2. Characterization of EGCG@BSP/HA MNs patches

In this study, we successfully prepared EGCG@BSP/HA MNs. The image shows that the EGCG@BSP/HA MNs array is 400 (20 × 20) (Fig. 2C). The optical microscope image (Fig. 2E) and the SEM image (Fig. 2D) show that the tip is cone-shaped, the tip is sharp and full, no bubbles, no hollowness, stable connection with the backing layer, no broken needle phenomenon, easy to insert into the skin. Due to the addition of DE powder, the uneven surface of the backing facilitates the adsorption of pus spilled as a result of microneedle puncture of the pustule. The 3D fluorescence images of EGCG@BSP/HA MNs were observed by CLSM (Fig. 2G, H). The bottom width was 400 nm, the height was 900 nm, and the distance between adjacent needles was 700 nm. FITC was distributed centrally at the tip of the needle, which facilitated drug delivery to the skin and avoided wastage. The content of EGCG in MNs was determined as 0.18 mg/patch by HPLC. In order to overcome the skin barrier, it is imperative for the needle to possess the mechanical strength to effectively pierce the skin. Hence, an examination of the mechanical characteristics of EGCG@BSP/HA MNs was conducted utilizing a texture analyzer. When subjected to external forces, MN undergoes deformation, resulting in the emergence of an inflection point on the force–displacement curve. Consequently, the force exerted on MN prior to this inflection point may be considered as its maximum bearing capacity. From the force–displacement curve (Fig. 2F), the maximum force that the EGCG@BSP/HA MNs can withstand is 0.54 N/needle. The above shows that we have successfully prepared EGCG@BSP/HA MNs and that they have sufficient strength to pierce the skin without causing damage [44,56].

3.3. Insertion test of EGCG@BSP/HA MNs

The in vitro insertion ability of EGCG@BSP/HA MNs was evaluated using Parafilm M® simulated skin. The findings indicated that the EGCG@BSP/HA MNs were able to effectively penetrate the Parafilm M® and reach the targeted layer (Fig. 3A). The depth of each layer was measured to be 100 nm, suggesting that the microneedles had the capability to penetrate up to a maximum depth of 500 nm. The perforation hole rates for layers 1, 2, 3, 4 and 5 were 100 %, 100 %, 91.3 %, 55.7 % and 22.7 %. According to prior research, it has been shown that the average thickness of the stratum corneum and dermis measures around 10–20 μm and 1–3 mm. Therefore, based on the puncture pore rate it is indicated that EGCG@BSP/HA MNs can successfully puncture the stratum corneum and form microchannels from the stratum corneum to the dermis, which facilitates the drug to reach the acne affected area.

To further evaluate the in vivo insertion properties of EGCG@BSP/HA MNs, we performed skin insertion experiments. Skin histology images show successful insertion of EGCG@BSP/HA MNs into the skin to a depth of 252 nm (Fig. 3C), which is necessary for in vivo efficacy experiments. The observed outcome is below the insertion depth threshold of 400 nm for the Parafilm M®. This discrepancy might perhaps be attributed to an offset phenomenon resulting from the skin's elastic properties [57].

3.4. Acute skin irritation test of EGCG@BSP/HA MNs and TEWL measurement

Through the figure, it can be seen that after removing the EGCG@BSP/HA MNs, the micro-needle holes in the skin were obvious and the skin was slightly reddened, but the puncture marks disappeared gradually with time, and finally disappeared within 50 min (Fig. 3D). There were no obvious irritation reactions (e.g., erythema, swelling, etc.) throughout the process, indicating that the EGCG@BSP/HA MNs could penetrate the skin and had good biocompatibility. In addition, when EGCG@BSP/HA MNs deliver drugs to lesions, EGCG@BSP/HA MNs produce only small holes that do not damage the skin [58].

The stratum corneum is a skin protective barrier, which can reduce the occurrence of external stimulation on the skin and maintain skin moisture to the maximum extent. The TEWL value, commonly known as the water loss value, is a typical indicator of the stratum corneum's barrier function. The TEWL value increased significantly after MNs were implanted under the skin, but it quickly went back to its initial level after 60 min (Fig. 3B) [59–61]. The TEWL value of the control group remained at about 16 g/ m^2h. The microchannels generated by EGCG@BSP/HA MNs disrupt the integrity of the stratum corneum, but microchannels can be rapidly closed. In general, MNs have the unique advantage of minimal skin irritation and rapid recovery. This suggests that MNs in transdermal drug delivery greatly improves the ease of administration and patient compliance.

3.5. In vivo dissolution of EGCG@BSP/HA MNs

As can be seen in the figure, EGCG@BSP/HA MNs inserted into the skin can rapidly dissolve and promote the release of the drug in the skin. In order to evaluate the solubility of EGCG@BSP/HA MNs in vivo, we removed EGCG@BSP/HA MNs from mouse skin at a specific time point [62]. The figure shows that the microneedle has not yet dissolved when it is not inserted into the skin of the mouse under the microscope. At this time, the needle tips are complete and sharp, and become blunt after 3 min of insertion. The needle tips are completely dissolved within 15 min (Fig. 3E). The results showed that EGCG@BSP/HA MNs could puncture the skin and the tip of the needle dissolved rapidly after contacting the tissue fluid, which was conducive to rapid transdermal drug delivery and improved patient compliance. Based on the solubility of EGCG@BSP/HA MNs, we left them on the mice skin for 15 min in subsequent in vivo experiments to fully dissolve and release the drug [44,63].

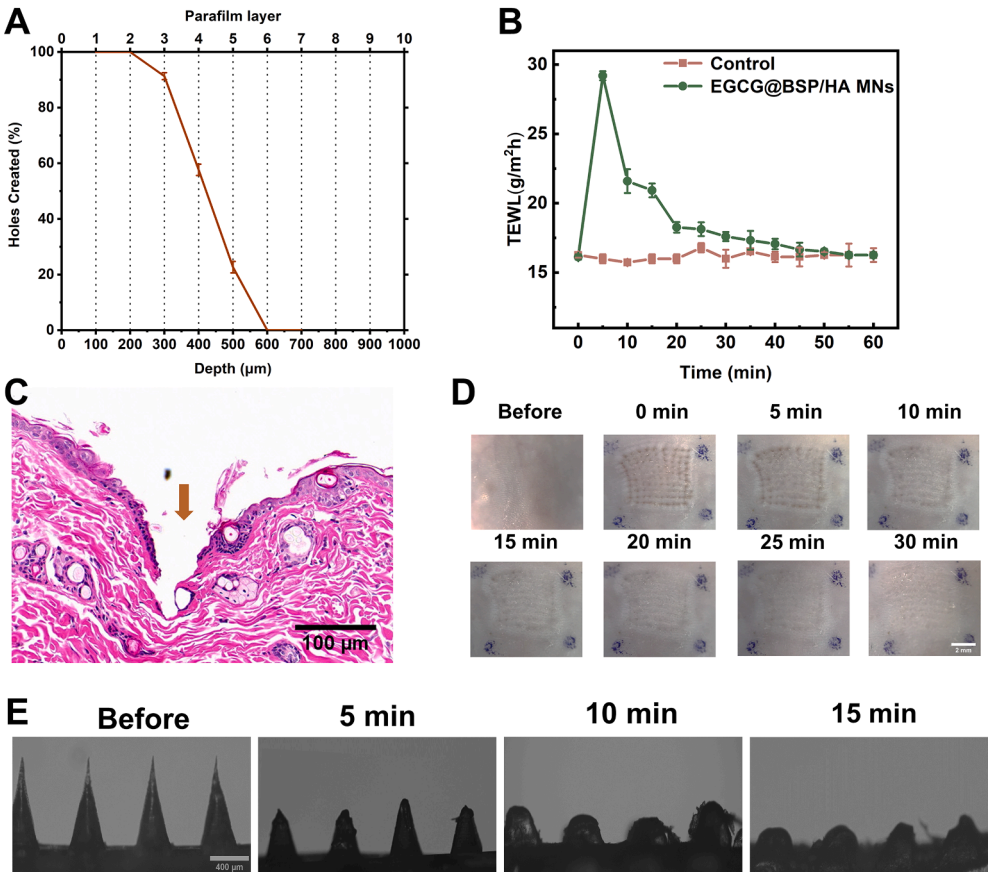

Fig. 3. Insertion test of EGCG@BSP/HA MNs. (A) Percentage of holes created and insertion depth of EGCG@BSP/HA MNs in Parafilm M® layers. (B) Effects of EGCG@BSP/HA MNs treatment on TEWL values of skin at specified time points compared with intact skin controls. (C) H&E staining of skin sections from following the application of EGCG@BSP/HA MNs for 5 min (Scale bar: 100 μm). (D) Photographs of EGCG@BSP/HA MNs-treated mice skin at different time intervals (Scale bar: 7 mm). (E) Dissolution of EGCG@BSP/HA MNs after their application onto mice skin in vivo at the indicated time points (Scale bar: 400 μm).

3.6. In vitro penetration depth study of EGCG@BSP/HA MNs

To visually assess the penetration depth of the medication into the skin, we prepared a soluble EGCG@BSP/HA MNs patch loaded with FITC and employed green fluorescence as a means to monitor and measure the penetration depth of the microneedle within the skin. Fluorescence images at different depths show that the fluorescence intensity becomes weaker as the scanning surface gets deeper [64]. The continuous fluorescence signal also indicates that the drug in the microneedle can diffuse rapidly into the skin. When the penetration depth is 360 nm, the green fluorescence disappears, indicating that this is the penetration depth of the microneedle (Fig. 4A). The depth of penetration of the microneedle was less than the tip height (900 nm), which may be due to the rapid dissolution of the tip of the microneedle during penetration and the deformation of the skin when the microneedle was inserted into the skin surface. In addition, the reconstructed 3D fluorescence images showed the shape from the stratum corneum to the epidermis in the shape of an inverted triangle, indicating that the drug could diffuse widely and rapidly in the skin.

3.7. In vitro transdermal delivery ability of EGCG@BSP/HA MNs

The mouse skin was immobilized on Franz to observe the in vitro transdermal delivery efficiency of EGCG through MNs (Fig. 4B). For comparison, we used a solution containing the same concentration of EGCG as the control. The figure shows the in vitro release profile of EGCG@BSP/HA MNs and EGCG solution. We can see that the release of the EGCG solution is very slow, with a cumulative release of less than 10 % after 24 h (Fig. 4C). The release of EGCG from the EGCG solution is very slow. This suggests that the EGCG solution does not readily penetrate the skin stratum corneum, which may be related to the skin barrier. EGCG was released in bursts in MNs, with a cumulative release of 60 % at 12 h and even up to 70 % in 24 h. However, due to the retention of the drug on the skin, the cumulative release is less than the amount of drug in the MNs. This result suggests that EGCG@BSP/HA MNs mediated transdermal drug delivery facilitates the penetration of the stratum corneum, which results in retention of the drug within the skin and slows down the transdermal rate of the drug. The ability of EGCG@BSP/HA MNs to maintain a high concentration of the drug in the skin over a long period of time facilitates sustained antimicrobial action for the treatment of acne vulgaris and reduces skin inflammation [44].

3.8. The hemolysis test of EGCG@BSP/HA MNs

We performed an in vitro hemolysis test on EGCG@BSP/HA MNs (Fig. 4D). As shown in the figure, the hemolysis rates of EGCG@BSP/HA MNs and BSP/HA MNs were 0.43 % and 0.83 % (Fig. 4E), respectively. According to the standard of biomedical materials (hemolysis rate < 5 %), both BSP/HA MNs and EGCG@BSP/HA MNs did not cause hemolysis, and their biocompatibility was in line with practical medical applications.

3.9. In vitro cytotoxicity of EGCG@BSP/HA MNs

The toxicity of microneedles solution to L929 cells was evaluated by the CCK-8 method. After 24 and 48 h of continuous culture, the EGCG@BSP/HA MNs 2 showed good biocompatibility (cell viability over 100 %) (Fig. S2A). The cell viability of L929 cells was >80 % after

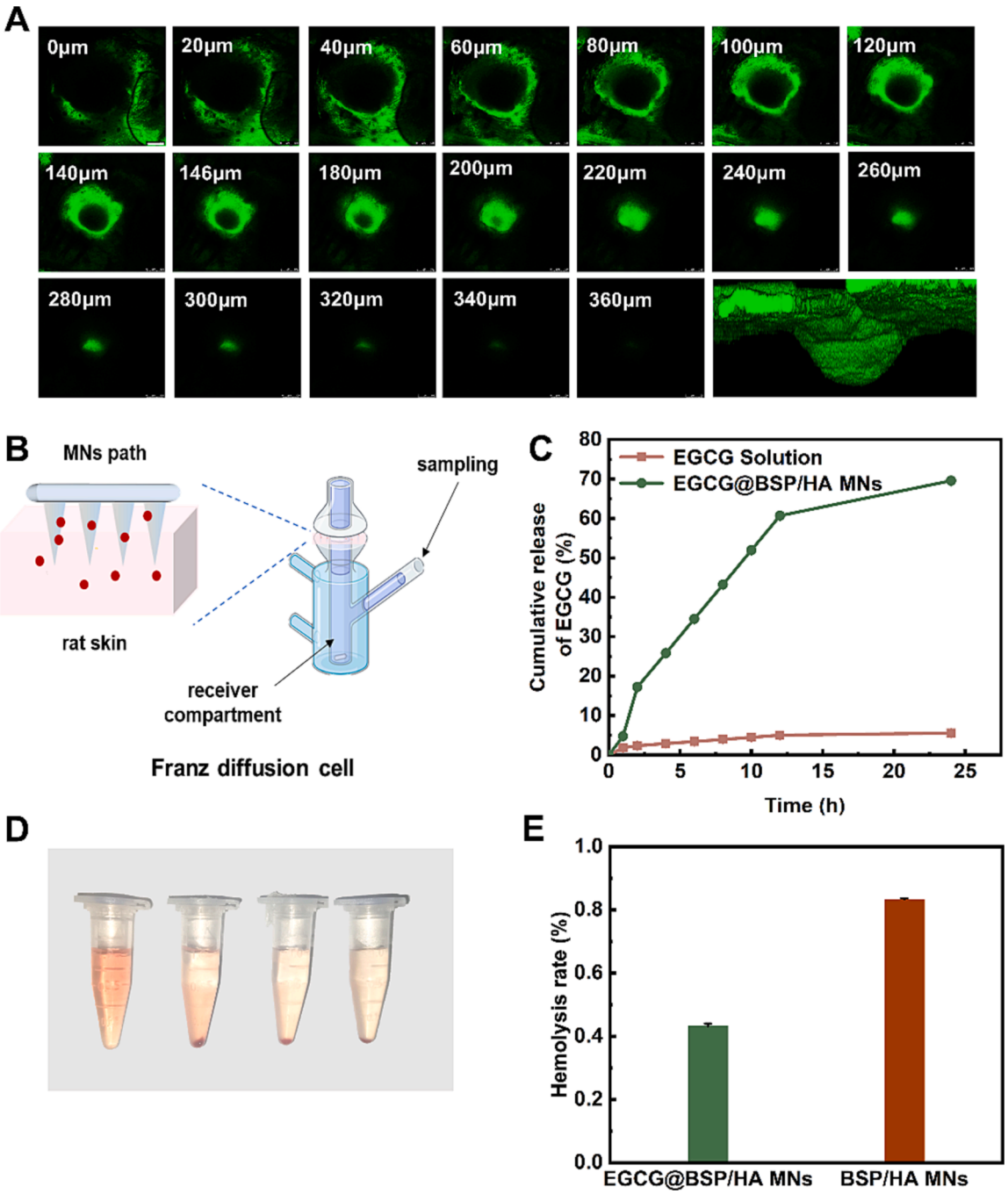

Fig. 4. In vitro skin penetration characterization of the EGCG@BSP/HA MNs. (A) Representation of the 3D micro-channels generated by the insertion of FITC loaded MNs. CLSM images of mice skin at varying depths. the penetration depth was from the skin surface to a depth of 360 μm (Scale bar: 200 μm). (B) Schematic illustration of Franz diffusion cell in the study of transdermal EGCG delivery. (C) In vitro permeation profile of EGCG through the mice skin from the MNs patch and EGCG Solution. Data is presented as mean ± SD (n = 4). (D) Photographs of hemolysis in EGCG@BSP/HA MNs and BSP/HA MNs. From left to right, positive control, BSP/HA MNs, EGCG@BSP/HA MNs and negative control. (E) Hemolysis rates for EGCG@BSP/HA MNs and BSP/HA MNs (n = 3).

48 h incubation with different concentrations of microneedle co-cultures (EGCG@BSP/HA MNs 1, EGCG@BSP/HA MNs 2, BSP/HA MNs). It indicated that small concentrations (0.25, 0.5, 1 mg/ mL) of microneedles also had a tendency to promote cell growth (Fig. S2B). The above results showed that EGCG@BSP/HA MNs 1, EGCG@BSP/HA MNs 2, and BSP/HA MNs had good cytocompatibility.

3.10. The adsorption properties of DE

The main component of diatomite is silicon dioxide. Scanning electron microscope (SEM) images show that DE has a porous structure (Fig. 5A), which indicates that it has adsorption capacity from the perspective of microstructure, and it is widely used as an absorbent [39,40]. The results showed that DE has excellent adsorption capacity for small molecules such as fluorescent dyes (Fig. 5B), and also has a stronger adsorption capacity for oil than AC (Fig. 5C). In summary,

diatomite can be used to adsorb acne pus and purulent exudates to reduce the risk of reinfection [41].

3.11. In vitro antibacterial effect of EGCG@BSP/HA MNs

The antimicrobial properties of EGCG@BSP/HA MNs were evaluated by the dilution-coated plate method (Fig. 6A) and the antibacterial rate was calculated. As shown, EGCG@BSP/HA MNs significantly reduced the survival of *S. aureus*, *E. coli* and *P. acnes* (Fig. 6B). And after 12 h of incubation, the inhibition rates of the loaded microneedles (MNs 1, MNs 2, MNs 3, MNs 4, MNs 5) with different EGCG concentrations were 20.70 %, 66.66 %, 75.40 %, 89.75 % and 97.06 % for *E. coli* (Fig. 6C), while at the same time the inhibition rates were 61.40 %, 76.32 %, 89.47 %, 93.29 % and 97.08 % against *S. aureus* (Fig. 6D). The inhibition rates of the drug-loaded microneedles against *P. acnes* after 48 h of incubation were 40.41 %, 66.57 %, 93.55 %, 97.95 % and 99.41 % (Fig. 6E). In summary, the antimicrobial effect of EGCG@BSP/HA MNs mainly depended on EGCG, and the higher the concentration of EGCG, the better the inhibitory effect. On this basis, the subsequent pharmacodynamic experiments were performed using the drug-loaded microneedles with EGCG (45 μg/patch).

In order to further understand the bactericidal effect based on EGCG@BSP/HA MNs, the bacterial morphology was observed by SEM (Fig. 7). As shown in the figure, after 24 h of incubation with EGCG@BSP/HA MNs in bacterial suspension, visibly dead bacteria were visible with irregular and unclear edges, collapsed surfaces, and shriveled or dissolved into fragments, suggesting that the bacterium had partially or completely ruptured the membrane. In the control group, *E. coli* and *P. acnes* were rod-shaped, *S. aureus* was spherical, and the surface remained smooth and complete. SEM images further confirmed the excellent antibacterial effect of EGCG@BSP/HA MNs, which can effectively inhibit *P. acnes* and other bacteria to treat acne.

The antimicrobial activity of each bacterial suspension was determined by measuring the optical density at 600 nm ($OD_{600\ nm}$) of each bacterial suspension after incubation with EGCG@BSP/HA MNs and commercial microneedles for 12 and 48 h (Fig. S3). The $OD_{600\ nm}$ values indicated that the untreated bacteria were in the logarithmic growth phase. Commercial microneedles were effective in inhibiting the proliferation of *S. aureus* and *P. acnes*, but had little or no inhibitory effect on *E. coli* when compared to the control group. The EGCG@BSP/HA MNs showed a good inhibitory effect on the above three bacteria, and was better than the commercial microneedles.

3.12. In vivo anti-acne experiments of EGCG@BSP/HA MNs

To evaluate the effect of EGCG@BSP/HA MNs patch on acne infection, we injected *P. acnes* intradermally into the backs of ICR mice to establish an acne model. As shown in the figure, on day 0 (after intradermal injection of *P. acnes*), about 0.5 mm thick acne formed at the injection site of *P. acnes* due to bacterial infection and proliferation, demonstrating the successful construction of the *P. acnes* infection acne model (Fig. 8A). Fig. 8B shows the treatment effect of each group on acne. To quantify the effect on acne treatment, acne thickness was measured during the treatment period (Fig. 8C), revealing changes in

Fig. 5. The adsorption properties of DE (A) SEM image of DE. (B) Adsorption capability of small molecular dye by DE. Adsorption of Rhodamine B (RhB) by different amount of DE in aqueous solution. (C) Oil adsorption test of DE. The DE or activated carbon (AC) adsorption of Rhodamine B (RhB) containing fatty acids (FA) with different weight ratios.

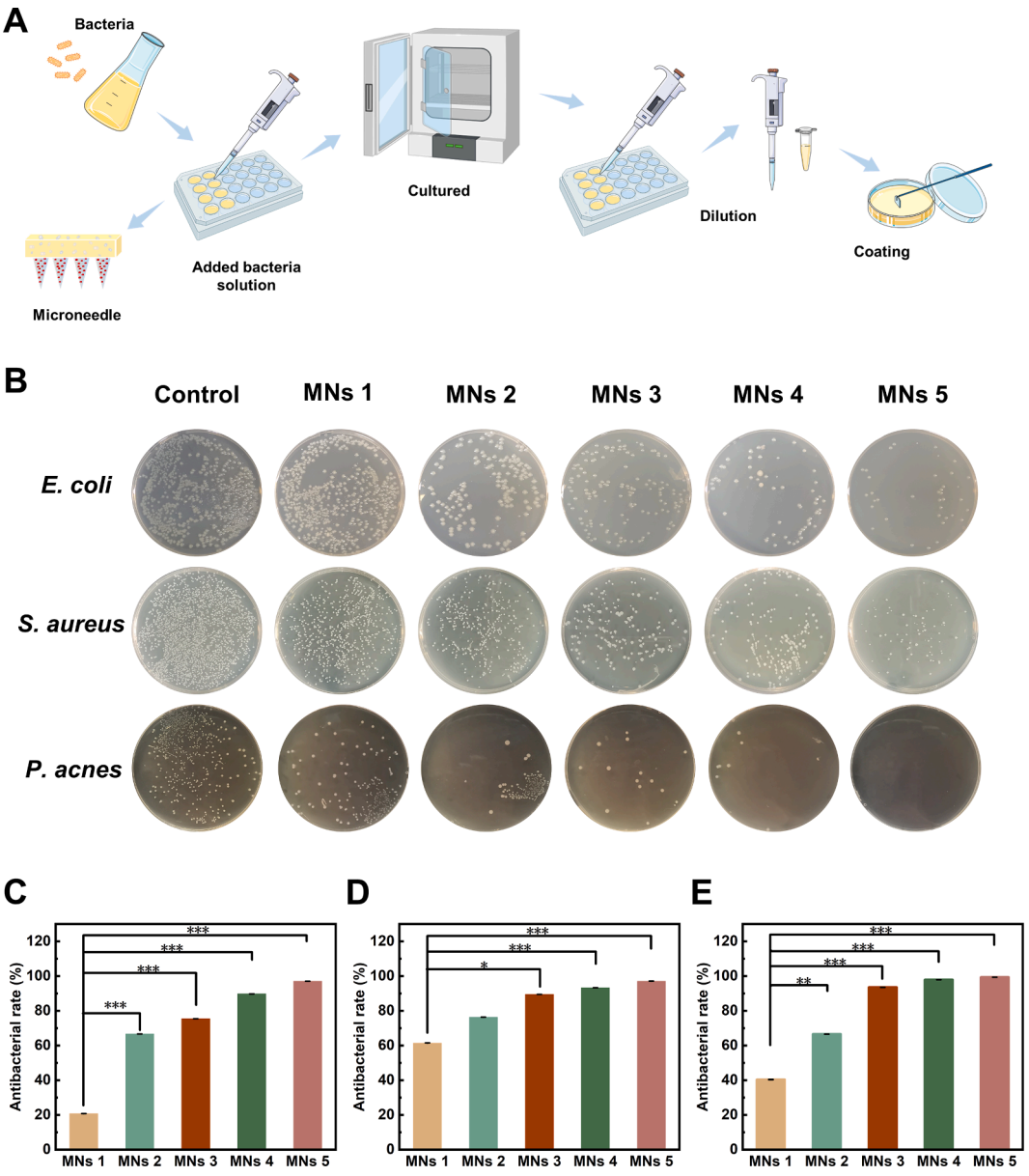

Fig. 6. In vitro antibacterial effect of EGCG@BSP/HA MNs. (A) Schematic diagram of antibacterial test. (B) Images of agar plates representing three colonies after microneedle treatment with different EGCG concentrations. (C) Bacteriostatic inhibition of *E. coli* after microneedles treatment with different EGCG concentrations. (D) Bacteriostatic inhibition of *S. aureus* after microneedles treatment with different EGCG concentrations. (E) Bacteriostatic inhibition of *P. acnes* after microneedles treatment with different EGCG concentrations. Data in Fig. 6C, D and E are presented as mean ± SD, n = 3 for each group; * $P < 0.05$, ** $P < 0.01$, *** $P < 0.001$.

acne thickness that was consistent with the treatment effect observed. The skin of the mice in the model group swelled without treatment until day 3, and the swelling was the most severe of the several groups. In contrast, after treatment with EGCG@BSP/HA MN, the skin thickness was significantly reduced, and some of the swelling even disappeared on day 8, indicating that EGCG@BSP/HA MNs patch has an effective inhibitory effect on acne growth. For BSP/HA MNs, which are not loaded with EGCG, their antibacterial effect is suboptimal although the needles are dissolved in the dermis, and they may have only a modest physical penetrating effect on acne. In the case of EGCG Solution, due to the absence of microneedle transdermal drug delivery and the presence of a skin barrier, it cannot effectively reach the sebaceous glands to exert its excellent antimicrobial activity, and may only have a slight antibacterial effect on acne. In addition, both the commercial microneedles group and the EGCG@BSP/HA MNs group showed good in vivo anti-acne when compared with the model group, and the therapeutic effect of EGCG@BSP/HA MNs was slightly better than that of commercial microneedles (Fig. S4).

To further evaluate the effect of EGCG@BSP/HA MNs on acne, mice were euthanized on day 8 and skin tissues were excised from the acne sites for histological and immunohistochemical analysis. H&E staining showed that the thickness of skin sections of EGCG@BSP/HA MNs group was thinner and free of pus sites than that of the other groups, which is consistent with the results of Fig. 9A. As shown in the × 40 H&E stained images, in the control group, the inflammatory cells in the subcutaneous tissue were densely distributed and the infiltration increased. In contrast, clear and intact reticular layers of dermal and follicular structures were observed in their skin tissues due to the good anti-infective properties of EGCG@BSP/HA MNs. *P. acnes* is an anaerobic Gram-positive bacteria [7,65]. Its excessive proliferation can stimulate sebaceous gland cells to synthesize sebum accumulation to block hair follicles, further leading to skin hypoxia and promoting bacterial growth. *P. acnes* infection can activate the NF-κB pathway and increase the expression of various cytokines, including TNF-α, IL-8, and MMP-2.

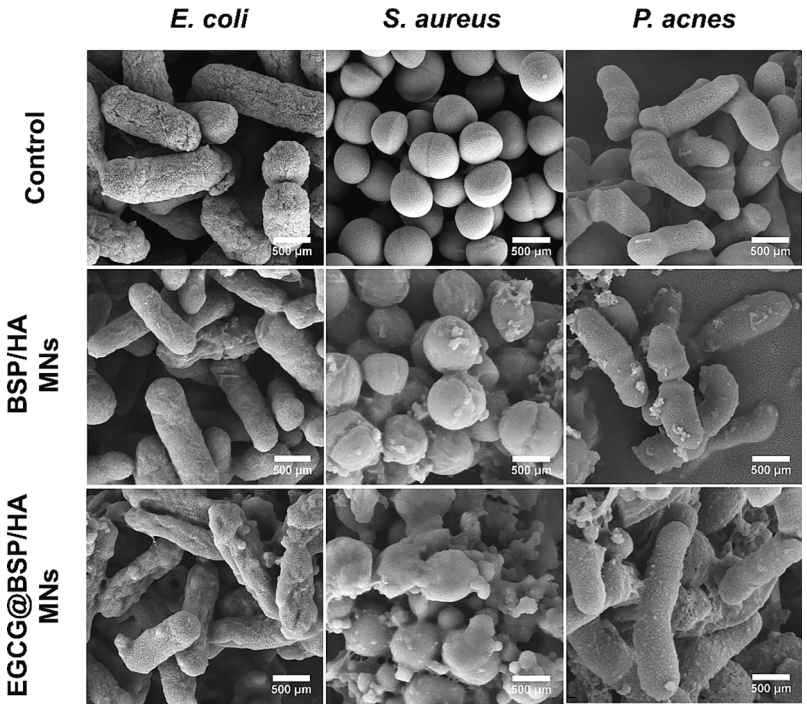

Fig. 7. SEM images displaying *E. coli*, *S. aureus* and *P. acnes* morphological changes during the antibacterial tests (Scale bar: 500 μm).

Obviously, both killing *P. acnes* and inhibiting the expression of cytokines can effectively treat acne [50]. Fig. 9B shows the distribution and expression of tumor necrosis factor-α (TNF-α), interleukin-8 (IL-8), and matrix metalloproteinase (MMP-2) in five groups of inflammatory cells and factors [50,55]. Compared with the control group, mice in the EGCG@BSP/HA MNs treatment group had the lowest expression of each inflammatory factor, and mice in the BSP/HA MNs and EGCG Solution treatment groups had relatively low expression of each inflammatory factor, which was consistent with the manifestation of individual acne infections in mice. It is proved again that EGCG@BSP/HA MNs has good

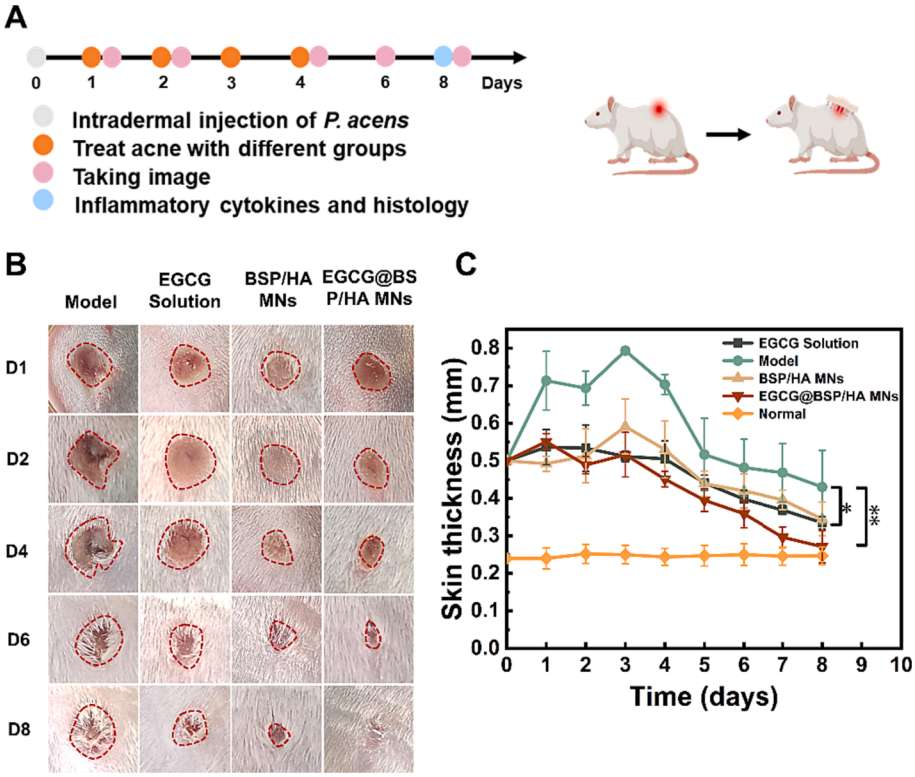

Fig. 8. In vivo anti-acne experiments of EGCG@BSP/HA MNs. (A) Schematic diagram of the establishment and treatment of *P. acnes* induced mice model. (B) Schematic representation of the skin acne therapy in a mouse model via topical EGCG@BSP/HA MNs, EGCG@BSP/HA MNs and EGCG Solution administration, (C) Thickness changes at acne in mice. * $P < 0.05$, ** $P < 0.01$, *** $P < 0.001$.; n = 5.

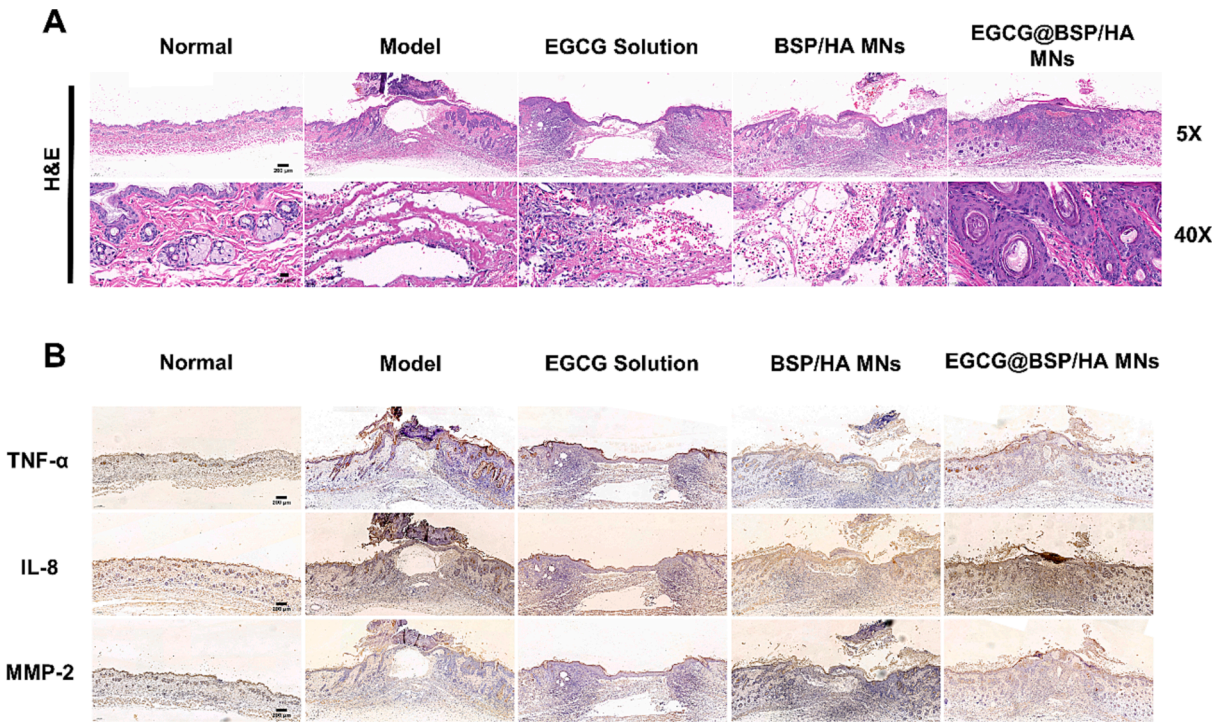

Fig. 9. (A) H&E skin slices. (n = 5, Scale bar: 200 μm). (B) Representative histological analyses of *P. acnes* -infected skin by immunohistochemical analysis of inflammatory factors from different group treated mice (Scale bar: 200 μm).

antibacterial and anti-inflammatory effects, can reduce the expression of inflammatory factors and proteins, and has a good therapeutic effect by combining the good healing effect of BSP.

4. Conclusion

In this study, a microneedle patch with BSP/HA loaded EGCG as the needle body material and PVA/DE as the backing material was prepared to obtain a novel and convenient acne drug delivery system. This system efficiently loads EGCG with sufficient mechanical strength to puncture the stratum corneum. In vitro transdermal experiments showed that EGCG administered by MNs could be retained in the skin for a long period of time with increased bioavailability. In addition, we found that EGCG@BSP/HA MNs had good antimicrobial properties and reduced the production of cytokines such as IL-8, TNF-α and MMP-2. The patch matrix containing PVA/DE also adsorbed pus and dead bacterial debris, accelerating skin healing, reduce the risk of reinfection, and ultimately ameliorating *P. acnes* induced acne in mice. In addition, EGCG@BSP/HA MNs transdermal administration of EGCG is virtually free of skin irritation and results in longer drug retention and better efficacy than EGCG solution alone. The microneedles in this study can also be used with other antimicrobial drugs. Thus, this study provides a reliable and easily expandable platform for the treatment of unusual acne. In summary, EGCG@BSP/HA MNs patches are expected to be an effective option for the treatment of acne vulgaris.

CRediT authorship contribution statement

Junbo Zhang: Investigation, Writing – original draft, Methodology, Visualization. **Peng Guo:** Validation, Writing – review & editing. **Mengyu Qiu:** Formal analysis, Software. **Guofeng Zhong:** Resources, Validation. **Qin Yang:** Resources, Software. **Pengkun Lei:** Software, Resources. **Kaijun Gou:** Data curation. **Rui Zeng:** Investigation, Supervision. **Chen Zhang:** Formal analysis, Writing – review & editing, Funding acquisition. **Yan Qu:** Conceptualization, Project administration.

Declaration of competing interest

The authors declare that they have no known competing financial interests or personal relationships that could have appeared to influence the work reported in this paper.

Data availability

The data that has been used is confidential.

Acknowledgments

The authors acknowledge Prof. Yan Qu and Dr. Chen Zhang for their discussions and suggestions during the preparation of this manuscript, as well as the support of Teacher Di Wang from the College of Pharmacy for the chemical composition analysis of this study. Thanks Shiyanjia Lab (www.shiyanjia.com) for the Biological SEM. This work was supported by Natural Science Foundation of Sichuan Province (2023NSFSC1768, 2023YFS0348), China Postdoctoral Science Foundation (2021M690488, 2023T160071), the Southwest Minzu University Research Startup Funds (No. RQD2023005, China), Innovation Team and Talents Cultivation Program of National Administration of Traditional Chinese Medicine (ZYYCXTD-D-202209), the Central Guidance on Local Science and Technology Development Fund of Sichuan (No. 2023ZYD0053, China).

Appendix A. Supplementary data

Supplementary data to this article can be found online at https://doi.org/10.1016/j.matdes.2024.112639.

References

[1] H.C. Williams, R.P. Dellavalle, S. Garner, Acne vulgaris, Lancet 379 (9813) (2012) 361–372.
[2] S. Cruz, N. Vecerek, N. Elbuluk, Targeting inflammation in acne: current treatments and future prospects, Am. J. Clin. Dermatol. 24 (5) (2023) 681–694.

[3] C.C. Zouboulis, A. Eady, M. Philpott, L.A. Goldsmith, C. Orfanos, W.C. Cunliffe, R. Rosenfield, What is the pathogenesis of acne? Exp. Dermatol. 14 (2) (2005) 143.
[4] I. Nagy, A. Pivarcsi, K. Kis, A. Koreck, L. Bodai, A. McDowell, H. Seltmann, S. Patrick, C.C. Zouboulis, L. Kemény, Propionibacterium acnes and lipopolysaccharide induce the expression of antimicrobial peptides and proinflammatory cytokines/chemokines in human sebocytes, Microbes Infect. 8 (8) (2006) 2195–2205.
[5] A.F. Bungau, A.-F. Radu, S.G. Bungau, C.M. Vesa, D.M. Tit, A.L. Purza, L.M. Endres, Emerging insights into the applicability of essential oils in the management of acne vulgaris, Molecules 28 (17) (2023).
[6] A.M. O'Neill, M.C. Liggins, J.S. Seidman, T.H. Do, F.W. Li, K.J. Cavagnero, T. Dokoshi, J.Y. Cheng, F. Shafiq, T.R. Hata, J.E. Gudjonsson, R.L. Modlin, R. L. Gallo, Antimicrobial production by perifollicular dermal preadipocytes is essential to the pathophysiology of acne, Sci. Transl. Med. 14 (632) (2022) 13.
[7] B. Dréno, S. Pécastaings, S. Corvec, S. Veraldi, A. Khammari, C. Roques, Cutibacterium acnes(Propionibacterium acnes) and acne vulgaris: a brief look at the latest updates, J. Eur. Acad. Dermatol. Venereol. 32 (2018) 5–14.
[8] C.C. Zouboulis, Acne as a chronic systemic disease, Clin. Dermatol. 32 (3) (2014) 389–396.
[9] A.L. Chien, J. Qi, B. Rainer, D.L. Sachs, Y.R. Helfrich, Treatment of acne in pregnancy, J. Am. Board Fam. Med. 29 (2) (2016) 254–262.
[10] R. Langasco, G. Spada, S.T. Tanriverdi, G. Rassu, P. Giunchedi, Ö. Özer, E. Gavini, Bio-based topical system for enhanced salicylic acid delivery: preparation and performance of gels, J. Pharm. Pharmacol. 68 (8) (2016) 999–1009.
[11] H.P. Tham, K. Xu, W.Q. Lim, H. Chen, M. Zheng, T.G.S. Thng, S.S. Venkatraman, C. Xu, Y. Zhao, Microneedle-Assisted topical delivery of photodynamically active mesoporous formulation for combination therapy of deep-seated melanoma, ACS Nano 12 (12) (2018) 11936–11948.
[12] T. Waghule, G. Singhvi, S.K. Dubey, M.M. Pandey, G. Gupta, M. Singh, K. Dua, Microneedles: a smart approach and increasing potential for transdermal drug delivery system, Biomed. Pharmacother. 109 (2019) 1249–1258.
[13] G. Ma, C. Wu, Microneedle, bio-microneedle and bio-inspired microneedle: a review, J. Control. Release 251 (2017) 11–23.
[14] M. Dalvi, P. Kharat, P. Thakor, V. Bhavana, S.B. Singh, N.K. Mehra, Panorama of dissolving microneedles for transdermal drug delivery, Life Sci. 284 (2021).
[15] Z. Sartawi, C. Blackshields, W. Faisal, Dissolving microneedles: applications and growing therapeutic potential, J. Control. Release 348 (2022) 186–205.
[16] C. Zhang, F. Gao, S. Gan, Y. He, Z. Chen, X. Liu, C. Fu, Y. Qu, J. Zhang, Chemical characterization and gastroprotective effect of an isolated polysaccharide fraction from Bletilla striata against ethanol-induced acute gastric ulcer, Food Chem. Toxicol. 131 (2019).
[17] T. Wen, Z. Lin, Y. Zhao, Y. Zhou, B. Niu, C. Shi, C. Lu, X. Wen, M. Zhang, G. Quan, C. Wu, X. Pan, Bioresponsive nanoarchitectonics-integrated microneedles for amplified chemo-photodynamic therapy against acne vulgaris, ACS Appl. Mater. Interfaces 13 (41) (2021) 48433–48448.
[18] D. Yang, M. Chen, Y. Sun, Y. Jin, C. Lu, X. Pan, G. Quan, C. Wu, Microneedle-mediated transdermal drug delivery for treating diverse skin diseases, Acta Biomater. 121 (2021) 119–133.
[19] R.C. Blasiak, C.R. Stamey, C.N. Burkhart, A. Lugo-Somolinos, D.S. Morrell, High-dose isotretinoin treatment and the rate of retrial, relapse, and adverse effects in patients with acne vulgaris, JAMA Dermatol. 149 (12) (2013).
[20] S.D. Crockett, C.Q. Porter, C.F. Martin, R.S. Sandler, M.D. Kappelman, Isotretinoin use and the risk of inflammatory bowel disease: a case-control study, Am. J. Gastroenterol. 105 (9) (2010) 1986–1993.
[21] M. Rademaker, Adverse effects of isotretinoin: a retrospective review of 1743 patients started on isotretinoin, Australas. J. Dermatol. 51 (4) (2010) 248–253.
[22] W. Cheng, F. Zhou, B. Zhu, X. Ding, J. Lu, C. Qian, X. Ye, Z. Ding, Characterization and evaluation of Bletilla striata polysaccharide/ethanol extract composite multifunctional sponges, Mater. Des. 206 (2021).
[23] Z.Y. Chen, L.Z. Cheng, Y.C. He, X.L. Wei, Extraction, characterization, utilization as wound dressing and drug delivery of Bletilla striata polysaccharide: a review, Int. J. Biol. Macromol. 120 (2018) 2076–2085.
[24] X. He, X. Wang, J. Fang, Z. Zhao, L. Huang, H. Guo, X. Zheng, Bletilla striata: medicinal uses, phytochemistry and pharmacological activities, J. Ethnopharmacol. 195 (2017) 20–38.
[25] J.X. Xiang, Y.J. Wang, L.P. Yang, X.J. Zhang, Y.L. Hong, L. Shen, A novel hydrogel based on Bletilla striata polysaccharide for rapid hemostasis: synthesis, characterization and evaluation, Int. J. Biol. Macromol. 196 (2022) 1–12.
[26] X. Ji, M. Yin, H. Nie, Y. Liu, A review of isolation, chemical properties, and bioactivities of polysaccharides from bletilla striata, Biomed Res. Int. 2020 (2020) 1–11.
[27] C. Chen, P. Zhou, C. Huang, R. Zeng, L. Yang, Z. Han, Y. Qu, C. Zhang, Photothermal-promoted multi-functional dual network polysaccharide hydrogel adhesive for infected and susceptible wound healing, Carbohydr. Polym. 273 (2021).
[28] L. Hu, Z. Liao, Q. Hu, K.G. Maffucci, Y. Qu, Novel Bletilla striata polysaccharide microneedles: fabrication, characterization, and in vitro transcutaneous drug delivery, Int. J. Biol. Macromol. 117 (2018) 928–936.
[29] Z. Liao, R. Zeng, L. Hu, K.G. Maffucci, Y. Qu, Polysaccharides from tubers of Bletilla striata: physicochemical characterization, formulation of buccoadhesive wafers and preliminary study on treating oral ulcer, Int. J. Biol. Macromol. 122 (2019) 1035–1045.
[30] Y. Qu, C. Li, C. Zhang, R. Zeng, C. Fu, Optimization of infrared-assisted extraction of Bletilla striata polysaccharides based on response surface methodology and their antioxidant activities, Carbohydr. Polym. 148 (2016) 345–353.
[31] G. Zhong, M. Qiu, J. Zhang, F. Jiang, X. Yue, C. Huang, S. Zhao, R. Zeng, C. Zhang, Y. Qu, Fabrication and characterization of PVA@PLA electrospinning nanofibers embedded with Bletilla striata polysaccharide and Rosmarinic acid to promote wound healing, Int. J. Biol. Macromol. 234 (2023).
[32] P. Zhou, S. Zhao, C. Huang, Y. Qu, C. Zhang, Bletilla striata polysaccharide microneedle for effective transdermal administration of model protein antigen, Int. J. Biol. Macromol. 205 (2022) 511–519.
[33] L. Chakrawarti, R. Agrawal, S. Dang, S. Gupta, R. Gabrani, Therapeutic effects of EGCG: a patent review, Expert Opin. Ther. Pat. 26 (8) (2016) 907–916.
[34] E. Kim, K. Hwang, J. Lee, S. Han, E.-M. Kim, J. Park, J. Cho, Skin protective effect of epigallocatechin gallate, Int. J. Mol. Sci. 19 (1) (2018).
[35] J. Steinmann, J. Buer, T. Pietschmann, E. Steinmann, Anti-infective properties of epigallocatechin-3-gallate (EGCG), a component of green tea, Br. J. Pharmacol. 168 (5) (2013) 1059–1073.
[36] M. Im, S.Y. Kim, K.C. Sohn, D.K. Choi, Y. Lee, Y.J. Seo, C.D. Kim, Y.L. Hwang, C. C. Zouboulis, J.H. Lee, Epigallocatechin-3-Gallate suppresses IGF-I-induced lipogenesis and cytokine expression in SZ95 sebocytes, J, Invest. Dermatol. 132 (12) (2012) 2700–2708.
[37] S. Saric, M. Notay, R. Sivamani, Green tea and other tea polyphenols: effects on sebum production and acne vulgaris, Antioxidants 6 (1) (2016).
[38] J.Y. Yoon, H.H. Kwon, S.U. Min, D.M. Thiboutot, D.H. Suh, Epigallocatechin-3-gallate improves acne in humans by modulating intracellular molecular targets and inhibiting P. acnes, J, Invest. Dermatol. 133 (2) (2013) 429–440.
[39] J. Delasoie, F. Zobi, Natural diatom biosilica as microshuttles in drug delivery systems, Pharmaceutics 11 (10) (2019).
[40] S. Maher, T. Kumeria, M.S. Aw, D. Losic, Diatom silica for biomedical applications: recent progress and advances, Adv. Healthc. Mater. 7 (19) (2018).
[41] Y. Zhang, P. Feng, J. Yu, J. Yang, J. Zhao, J. Wang, Q. Shen, Z. Gu, ROS-responsive microneedle patch for acne vulgaris treatment, Advanced Therapeutics 1 (3) (2018).
[42] L. Yang, Z. Han, C. Chen, Z. Li, S. Yu, Y. Qu, R. Zeng, Novel probiotic-bound oxidized Bletilla striata polysaccharide-chitosan composite hydrogel, Mater. Sci. Eng. C 117 (2020).
[43] X. Yue, S. Zhao, M. Qiu, J. Zhang, G. Zhong, C. Huang, X. Li, C. Zhang, Y. Qu, Physical dual-network photothermal antibacterial multifunctional hydrogel adhesive for wound healing of drug-resistant bacterial infections synthesized from natural polysaccharides, Carbohydr. Polym. 312 (2023).
[44] C. Huang, K. Gou, X. Yue, S. Zhao, R. Zeng, Y. Qu, C. Zhang, A novel hyaluronic acid-based dissolving microneedle patch loaded with ginsenoside Rg3 liposome for effectively alleviate psoriasis, Mater. Des. 224 (2022).
[45] C. Salamanca, A. Barrera-Ocampo, J. Lasso, N. Camacho, C. Yarce, Franz diffusion cell approach for pre-formulation characterisation of ketoprofen semi-solid dosage forms, Pharmaceutics 10 (3) (2018).
[46] P.W.R. Ananda, D. Elim, H.S. Zaman, W. Muslimin, M.G.R. Tunggeng, A. D. Permana, Combination of transdermal patches and solid microneedles for improved transdermal delivery of primaquine, Int. J. Pharm. 609 (2021).
[47] R. Luo, L. Tang, S. Zhong, Z. Yang, J. Wang, Y. Weng, Q. Tu, C. Jiang, N. Huang, In vitro investigation of enhanced hemocompatibility and endothelial cell proliferation associated with quinone-rich polydopamine coating, ACS Appl. Mater. Interfaces 5 (5) (2013) 1704–1714.
[48] M. Qiu, G. Zhong, J. Zhang, Y. Hou, Y. Duan, P. Guo, F. Jiang, K. Gou, C. Zhang, Y. Qu, Biocompatible and biodegradable Bletilla striata polysaccharides hydrogels crosslinked by BDDE for wound healing through the regulating of macrophage polarization, Int. J. Biol. Macromol. 254 (2024).
[49] F. Jiang, X. Li, Y. Duan, Q. Li, Y. Qu, G. Zhong, M. Qiu, J. Zhang, C. Zhang, X. Pan, Extraction and characterization of chitosan from Eupolyphaga sinensis Walker and its application in the preparation of electrospinning nanofiber membranes, Colloids Surf. B Biointerfaces 222 (2023).
[50] T. Zhang, B. Sun, J. Guo, M. Wang, H. Cui, H. Mao, B. Wang, F. Yan, Active pharmaceutical ingredient poly(ionic liquid)-based microneedles for the treatment of skin acne infection, Acta Biomater. 115 (2020) 136–147.
[51] J. Qin, M. Li, M. Yuan, X. Shi, J. Song, Y. He, H. Mao, D. Kong, Z. Gu, Gallium(III)-mediated dual-cross-linked alginate hydrogels with antibacterial properties for promoting infected wound healing, ACS Appl. Mater. Interfaces 14 (19) (2022) 22426–22442.
[52] D. Li, Y. Sun, X. Ren, N. Zhou, L. Li, G. He, S. Ma, Y. Wang, Dynamic evaluation of pathological changes in a mouse acne model by optical imaging technology, Exp. Dermatol. 32 (9) (2023) 1350–1360.
[53] A. Rimon, C. Rakov, V. Lerer, S. Sheffer-Levi, S.A. Oren, T. Shlomov, L. Shasha, R. Lubin, K. Zubeidat, N. Jaber, M. Mujahed, A. Wilensky, S. Coppenhagen-Glazer, V. Molho-Pessach, R. Hazan, Topical phage therapy in a mouse model of Cutibacterium acnes-induced acne-like lesions, Nat Commun 14 (1) (2023).
[54] S.L. Kolar, C.-M. Tsai, J. Torres, X. Fan, H. Li, G.Y. Liu, Propionibacterium acnes–induced immunopathology correlates with health and disease association, JCI Insight 4 (5) (2019).
[55] Y.M. Xiang, J.L. Lu, C.Y. Mao, Y.Z. Zhu, C.F. Wang, J. Wu, X.M. Liu, S.L. Wu, K.Y. H. Kwan, K.M.C. Cheung, K.W.K. Yeung, Ultrasound-triggered interfacial engineering-based microneedle for bacterial infection acne treatment, Sci. Adv. 9 (10) (2023).
[56] P. Zhou, C. Chen, X. Yue, J. Zhang, C. Huang, S. Zhao, A. Wu, X. Li, Y. Qu, C. Zhang, Strategy for osteoarthritis therapy: improved the delivery of triptolide using liposome-loaded dissolving microneedle arrays, Int. J. Pharm. 609 (2021).
[57] S. Cao, Y. Wang, M. Wang, X. Yang, Y. Tang, M. Pang, W. Wang, L. Chen, C. Wu, Y. Xu, Microneedles mediated bioinspired lipid nanocarriers for targeted treatment of alopecia, J. Control. Release 329 (2021) 1–15.

[58] Y.-H. Chiu, Y.-W. Wu, J.-I. Hung, M.-C. Chen, Epigallocatechin gallate/L-ascorbic acid–loaded poly-γ-glutamate microneedles with antioxidant, anti-inflammatory, and immunomodulatory effects for the treatment of atopic dermatitis, Acta Biomater. 130 (2021) 223–233.
[59] H. Alexander, S. Brown, S. Danby, C. Flohr, Research techniques made simple: transepidermal water loss measurement as a research tool, J. Invest. Dermatol. 138 (11) (2018) 2295–2300.e1.
[60] M.F. Galliano, A. Tfayli, R.H. Dauskardt, B. Payre, C. Carrasco, S. Bessou-Touya, A. Baillet-Guffroy, H. Duplan, Comprehensive characterization of the structure and properties of human stratum corneum relating to barrier function and skin hydration: modulation by a moisturizer formulation, Exp. Dermatol. 30 (9) (2021) 1352–1357.
[61] F. Netzlaff, K.-H. Kostka, C.-M. Lehr, U.F. Schaefer, TEWL measurements as a routine method for evaluating the integrity of epidermis sheets in static franz type diffusion cells in vitro limitations shown by transport data testing, European Journal of Pharmaceutics and Biopharmaceutics 63 (1) (2006) 44–50.
[62] P. Li, C.H. Liu, Y.Y. Zhao, D.D. Cao, B.Z. Chen, X.D. Guo, W.F. Zhang, Multifunctional covalent organic framework-based microneedle patch for melanoma treatment, Biomacromolecules (2023).
[63] N. Zhang, L. Xue, A. Younas, F. Liu, J. Sun, Z. Dong, Y. Zhao, Co-delivery of triamcinolone acetonide and verapamil for synergistic treatment of hypertrophic scars via carboxymethyl chitosan and Bletilla striata polysaccharide-based microneedles, Carbohydr. Polym. 284 (2022).
[64] H. Du, P. Liu, J. Zhu, J. Lan, Y. Li, L. Zhang, J. Zhu, J. Tao, Hyaluronic acid-based dissolving microneedle patch loaded with methotrexate for improved treatment of psoriasis, ACS Appl. Mater. Interfaces 11 (46) (2019) 43588–43598.
[65] A.B. Salinas, Acne vulgaris: role of the immune system, Int. J. Dermatol. 60 (9) (2021) 1076–1081.